


Article

# Parametric Testing of Metasurface Stirrers for Metasurfaced Reverberation Chambers

Hengyi Sun <sup>1,2</sup>, Changqing Gu <sup>1,\*</sup>, Zhuo Li <sup>1</sup>, Qian Xu <sup>1</sup>, Mengmeng Wei <sup>3</sup>, Jiajia Song <sup>1</sup>,  
Baijie Xu <sup>1</sup>, Xiaohang Dong <sup>1</sup>, Kuan Wang <sup>1</sup> and Ferran Martín <sup>2,\*</sup> 

<sup>1</sup> Key Laboratory of Radar Imaging and Microwave Photonics, Ministry of Education, College of Electronic and Information Engineering, Nanjing University of Aeronautics and Astronautics, Nanjing 211106, China; lizhuo@nuaa.edu.cn (Z.L.); emxu@foxmail.com (Q.X.); JJSNUAA@foxmail.com (J.S.); xbj12123@outlook.com (B.X.); dongxiaohang@hotmail.com (X.D.); kuanwang@nuaa.edu.cn (K.W.)

<sup>2</sup> CIMITEC, Departament d'Enginyeria Electrònica, Universitat Autònoma de Barcelona, 08193 Bellaterra, Barcelona, Spain; hengyi.sun@e-campus.uab.cat

<sup>3</sup> College of Humanities & Social Development, Northwest A&F University, Yangling 712100, China; 18291892319@163.com

\* Correspondence: gucq@nuaa.edu.cn (C.G.); ferran.martin@uab.cat (F.M.)

Received: 14 January 2019; Accepted: 19 February 2019; Published: 25 February 2019



**Abstract:** In this paper, the correlation coefficients and the total scattering cross sections (TSCSs) for different types of metasurfaced stirrers and the traditional metallic stirrer, and the effects on field uniformity when such stirrers are used in reverberation chambers, are analyzed. Three metasurfaced stirrers are considered: A stirrer with two unit cells arranged alternatively (#1), a stirrer with two unit cells arranged in a chessboard-like manner (#2), and a stirrer with two unit cells in random arrangement (#3). From the correlation coefficient and TSCS results obtained in simulations, it follows that metasurfaced stirrer #1 is the best option. Field uniformity analysis of the resulting metasurface reverberation chambers (MRC) equipped with the different stirrers also supports this conclusion.

**Keywords:** metasurface; reverberation chamber; stirrer; field uniformity

## 1. Introduction

In general, a reverberation chamber (RC) consists of a metal shielded chamber containing stirrers, antennas, a piece of equipment under test, as well as other devices. Formally, an RC can be defined as an electrically large, high quality factor (Q), multimode cavity that uses mode stirring to create changing boundary conditions in order to obtain a statistically uniform electromagnetic field [1,2]. RCs, also called mode-stirred chambers, are common test facilities widely used for electromagnetic compatibility (EMC) measurements, multipath environment characterization, electromagnetic immunity analysis, power radiation estimation, etc. [3].

In the past, many efforts have been focused on trying to optimize the performance of metallic stirrers in conventional RCs. Mainly through the application of empirical techniques and common sense, heuristic guides, which define and adopt many design criteria, have been proposed. For instance, stirrers should be greater than or equal to the wavelength of the lowest usable frequency (LUF), stirrers should be shaped such that a non-repeating field pattern is obtained in one rotation, etc. In this sense, references [3–11] provide some practical contributions to stirrer design and stirrer optimization, and there are examples of flexible stirrers that optimize RC performance by selecting the optimum angle of the bend [5,6], the position of the stirrer blades [7,8], or the independent number of the stirrer positions [9,10].

Despite the efforts directed towards stirrer optimization, certain limitations and constraints arise in real-life scenarios (e.g., large stirrers penalize the available test volume; complex stirrer shapes may hinder

the design and implementation, thereby increasing costs). To date, few efforts have been concentrated on alternative stirring methods which may provide a solution to the previous limitative aspects. In this regard, the concept of a metasurfaced reverberation chamber (MRC), with stirrers based on metasurfaces, has been recently proposed [11] as an alternative to conventional RCs. Metasurfaces are the planar counterparts of metamaterials, consisting of a single-layer or few-layer stack of planar structures, which can be fabricated using lithography and nanoprinting methods, and are usually described by effective medium parameters at the macroscopic scale; see [11,12].

In [11], we used a 1-bit random coding metasurface to realize the MRC. The 1-bit random coding diffusion metasurface was designed in order to obtain all-direction backscattering under normal incidence. By rotating the metasurface stirrer, wave diffusion (at least in the transient electromagnetic field distribution) is ensured. Moreover, such a metasurface is not only a specific mode tuner, but also a phase wall with multiple boundary conditions. Thus, the mode structure changes at each stir state. The main conclusion in [11] was that although the field uniformity was only somewhat improved for the MRC with the rotating 1-bit coding diffusion metasurface (as compared to the traditional one), an extended MRC test zone was achieved due to the lack of mechanical stirrer. In [13], we analyzed the physical mechanism for increasing the number of modes, lowering the operating frequency, and improving the field uniformity in the reverberation chambers, and concluded that a designed sequential metasurface provided better stirring effect than the random one. After dealing with these studies, it is concluded that the coding metasurface stirrer can improve the uniformity of field distribution in the MRC, and can replace the traditional metallic stirrer. Moreover, using metasurface walls in the chamber is useful to increase the number of modes and to lower the useful frequency, especially for the metasurface with unit cells arranged alternatively [13].

In this work, we study and compare three different types of rotating metasurfaced stirrer (also including the mechanical metallic stirrer in the comparison) on the basis of their influence on RC performance. The key performance indicators are the correlation coefficients and total scattering cross section (TSCS).

### 1.1. Simulation Parameters Set Up

The simulated RC was 1.2 m long, 0.8 m wide, and 1.2 m high, with a transmitting antenna as shown in Figure 1. The dimensions of the antenna and the simulation of the reflection coefficient in free space are also depicted in Figure 1 (the orientation of the antenna had no effect on simulation results, as it had been corroborated from independent results (not shown)). In our case, the distance of the boundary of test volume to the wall of the RC was  $\lambda = 0.375$  m, where  $\lambda$  was the wavelength of the LUF (800 MHz, in our case, where the number of modes of the RC was above 100). It was at least half a meter from all other metallic surfaces and it remained the same for all the simulated configurations, for the sake of comparison, even though for some analyzed configurations it could have been greater.

The considered metasurfaced stirrers in the present study were based on two types of unit cells, with “0” and “ $\pi$ ” phase responses to mimic the “0” and “1” elements of the 1-bit digital coding metasurface (these can be controlled using existing digital technology [14]). The details of the unit cell are described in [11]. With such unit cells, we designed three different metasurfaced stirrers, which were compared with each other and with the metallic stirrer. The metasurfaced stirrers contained (i) two unit cells arranged alternatively (#1), (ii) two unit cells arranged in a chessboard-like manner (#2), and (iii) two unit cells in random arrangement (#3). By following the concept of coding metamaterial, case #1 was characterized by coding sequences 0101 ... /0101 ... , case #2 by coding sequences 0101 ... /1010 ... , and case #3 was the 1-bit random coding case (Figure 2).

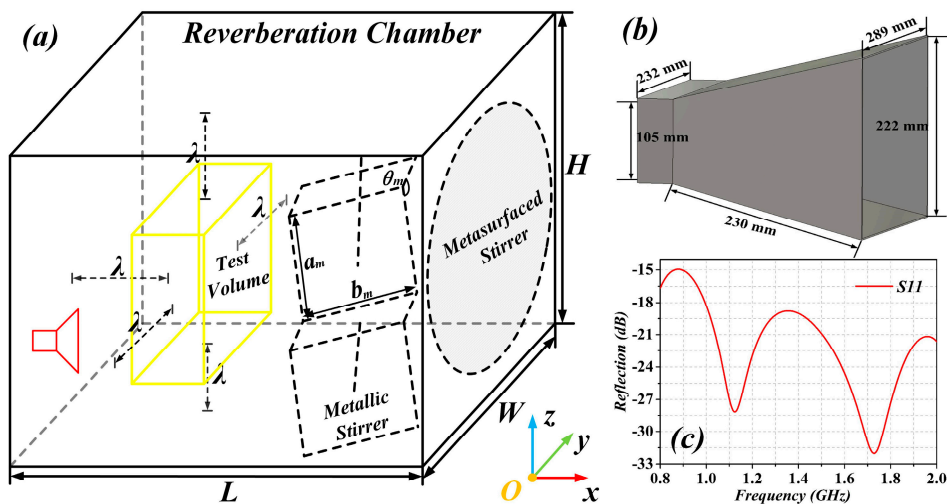


**Figure 1.** Schematic diagram of the reverberation chamber (RC) with metallic stirrer or with metasurfaced stirrer (a), three-dimensional view of the antenna (b), and its reflection coefficient (c).  $L = 1.2$  m,  $W = 0.8$  m and  $H = 1.2$  m. Dimensions of the metallic stirrer were  $a_m = 0.3$  m,  $b_m = 0.4$  m,  $\theta_m = 120^\circ$  and the thickness of all the metallic blades was 2 mm. The diameter of the metasurfaced stirrer was 1.2 m, and the considered dielectric layer was 0.031 m thick, with dielectric constant  $\epsilon_r = 2.65$  and loss tangent  $\tan\delta = 0.001$ .

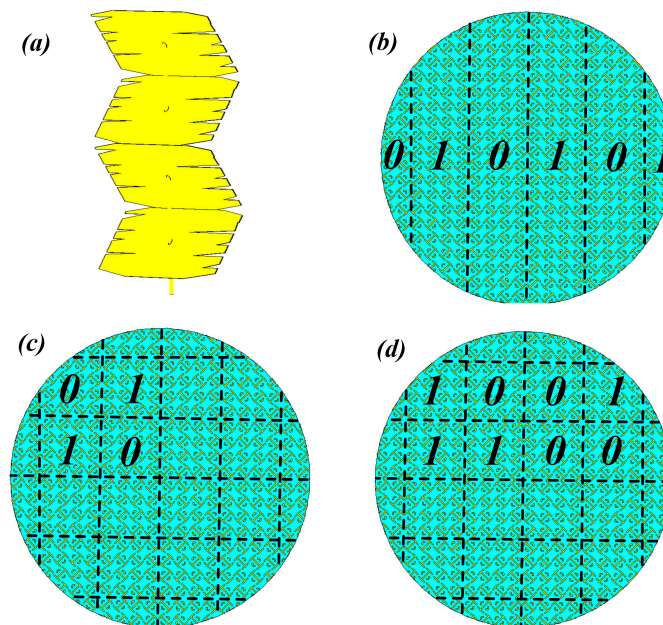


**Figure 2.** Metallic stirrer (a), periodic metasurfaced stirrer with coding sequences 0101... /0101... (b) and 0101... /1010... (c), and 1-bit random coding metasurfaced stirrer (d).

In order to analyze the scattering characteristic of the stirrers, we first simulated the far-field pattern of the stirrers by means of CST Microwave Studio<sup>®</sup> (CST China Ltd. Nanjing, China). The different stirrers generated a diffuse far-field scattering pattern, as depicted in Figure 3. The pattern obtained by full-wave simulation was in agreement with the result of the optimization algorithm [14]. In the CST software, we set the maximum number of cells per wavelength to 20, both in near- and far-form model options.

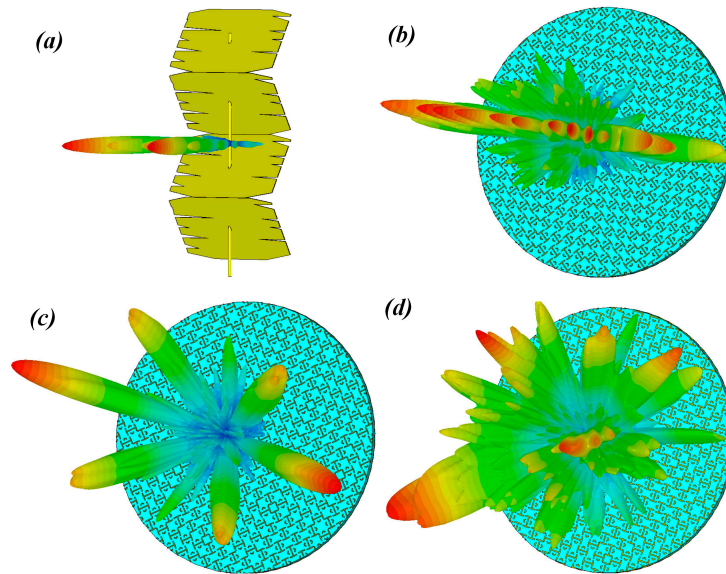


**Figure 3.** Simulated far-field pattern of the metallic stirrer (a) and metasurfaced stirrers (b) #1, (c) #2, and (d) #3 under normal incidence at 1 GHz (excitation with a plane wave is considered).

### 1.2. Analysis of Simulation Results

To evaluate whether a stirrer provides independent field conditions for the different rotation positions, the correlation coefficient is the key parameter. It is assumed that uncorrelated stirrer positions yield independent field conditions [15]. Thus, the correlation coefficient between different three-dimensional far-field patterns of the metasurface corresponding to different rotation angles, as introduced in [11], was calculated. The correlation coefficients with the variations of the rotation angle from  $0^\circ$  to  $45^\circ$  in steps of  $3^\circ$  are shown in Figure 4. In the diagram, it can be observed that the correlation coefficients of stirrers #1 and #3 decrease sharply within 10 degrees of the rotation angle. This decrease in the correlation coefficient is indicative of the different electric field patterns between the different angles (due to changing boundary conditions), giving rise to an effective improvement of field uniformity.

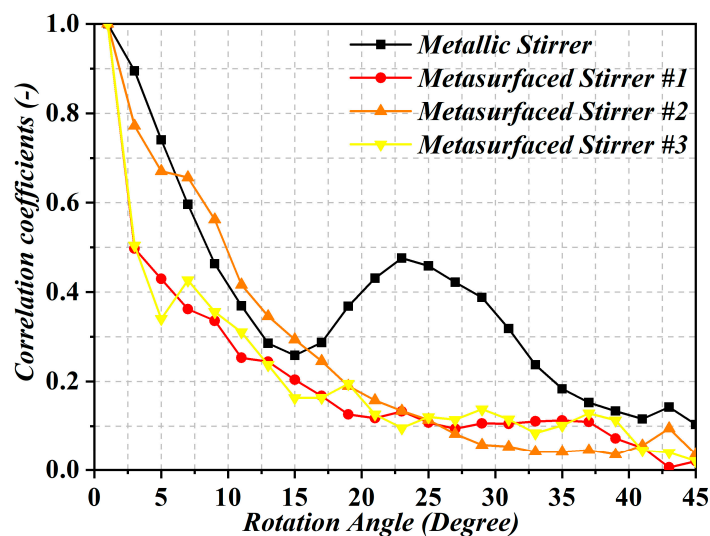


**Figure 4.** Correlation coefficients of the metallic and metasurfaced stirrers at 1 GHz.

The TSCS reveals an interesting criterion to quantify the target scattering ability. In the EMC regard, the TSCS of an RC provides an indication of the capability of the chamber to generate statistical



field uniformity, through stirring efficiency [16–20]. To compute the TSCS in a reverberant environment, the commercial software CST Microwave Studio<sup>®</sup> (CST China Ltd. Nanjing, China) was employed. Nevertheless, the theoretical foundations of TSCS are given as follows. The expression giving the mean value of the E-field  $E_\eta(t)$  ( $\eta = x, y, z$ : Cartesian component) over the sources  $\alpha$  (in our case,  $\alpha = 1$ ), probes  $\beta$  (in our case,  $\beta = 8$ ) and over the various object locations  $\gamma$  (in our case,  $\gamma = 1$ ) at time  $t$ , is as follows [18,21]:

$$\left\langle \left\langle E_\eta(t) \right\rangle_\gamma^2 \right\rangle_{\alpha,\beta} = \left\langle \left\langle E_\eta(t=0) \right\rangle_\gamma^2 \right\rangle_{\alpha,\beta} e^{-t/\tau_s}. \quad (1)$$

The TSCS can be inferred from the scattering damping time  $\tau_s$ :

$$TSCS = V/N\tau_s c, \quad (2)$$

where  $V$  is the volume of the chamber,  $N$  is the number of moving objects (in our case,  $N = 1$ ) and  $c$  is the speed of light in vacuum. After rewriting (1), we can define the ratio  $C(t)$  as follows:

$$C(t) = \frac{\left\langle \left\langle E_\eta(t) \right\rangle_\gamma^2 \right\rangle_{\alpha,\beta}}{\left\langle \left\langle E_\eta^2(t=0) \right\rangle_\gamma \right\rangle_{\alpha,\beta,\gamma}} = e^{-t/\tau_s}. \quad (3)$$

Therefore, the scattering damping time  $\tau_s$  can be linearly derived from relations (1) and (3) according to:

$$\tau_s = -\frac{t}{\ln[C(t)]}, \quad (4)$$

where  $C(t)$  is inferred through the CST simulation.

In Figure 5, we plotted  $\ln C(t)$  corresponding to the four stirrers (#1, #2, #3, and the metallic stirrer). After the estimation of the damping time ( $\tau_s$ ), the TSCS was computed for the four stirrers (TSCS is inversely proportional to  $\tau_s$ , according to Expression 2). Note that for a high Q cavity, waves outperform many bounces within the cavity before they decay. Thus, the higher the Q value, the longer the  $\tau_s$  [22]. In other words, small  $\tau_s$  is associated with significant stirring. From the results of Figure 5, it can be clearly seen that  $\ln C(t)$  of stirrers #1 and #3 reduces sharply, as compared to the metallic stirrer and stirrer #2. In other words, the stirrers #1 and #3 exhibited better TSCS and stirring efficiency. Note that  $\tau_s$  can be extracted from the least-square fit of the logarithm of  $C(t)$  in (3) [23,24], thus, the TSCS can be obtained using expression (2) (signals after 100  $\mu$ s are the noise floor and are not used for the least-square fit). The stirrer was rotated through 12 stirrer positions (30 degrees/step). The values of TSCS for the four considered cases were found to be: 0.168 m<sup>2</sup> (metallic stirrer), 0.195 m<sup>2</sup> (metasurface stirrer #1), 0.123 m<sup>2</sup> (metasurface stirrer #2), 0.189 m<sup>2</sup> (metasurface stirrer #3).

To further verify our optimization results for the metasurfaced stirrers, some standard EMC tests [25] were carried out for the four stirrers. Particularly, the E-field components were recorded by isotropic probes placed on the eight corners of the test volume. According to [25], and taking into account the LUF of our metasurfaced reverberation chamber configuration and the studied bandwidth, the simulations were repeated for 12 steps of the stirrer rotation. The uniformity and the isotropy of the E-field are defined as the standard deviation with respect to the mean value of the maximum measures obtained for each of the eight probes and for a complete rotation of the stirrer. The results are shown in Figure 6. In the figure, the acceptable limits for field uniformity decreed in [25] are within 3 dB above 400 MHz. We plotted the standard deviation calculated from the mean value of the maximum E-field by giving equal weight to each component. The average values of the standard deviation were 2.06 dB, 1.81 dB, 2.63 dB, and 1.93 dB for the metallic stirrer and metasurfaced stirrers (#1, #2, #3), respectively. Thus, metasurfaced stirrer #1 provided a greater scattering efficiency compared to the others. We note that metasurfaced stirrer #1 respected the tolerance constraint, in accordance with the results of correlation coefficient and TSCS. From all these results, we can conclude that metasurfaced stirrer #1 exhibited much better stirring efficiency.

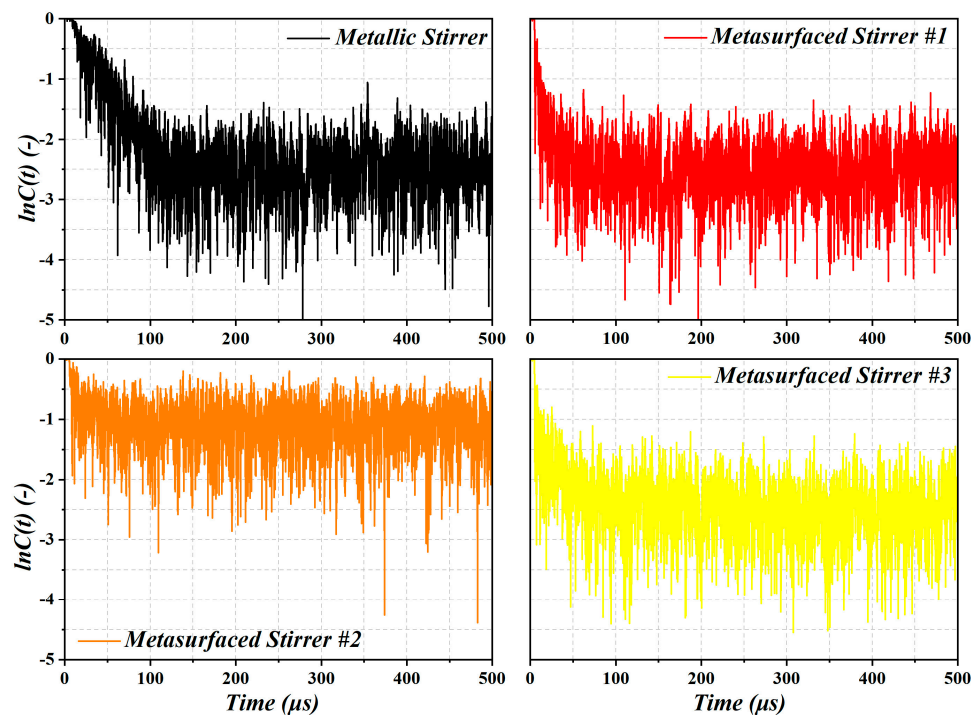


Figure 5. A comparison of the C ratio between the four stirrers.

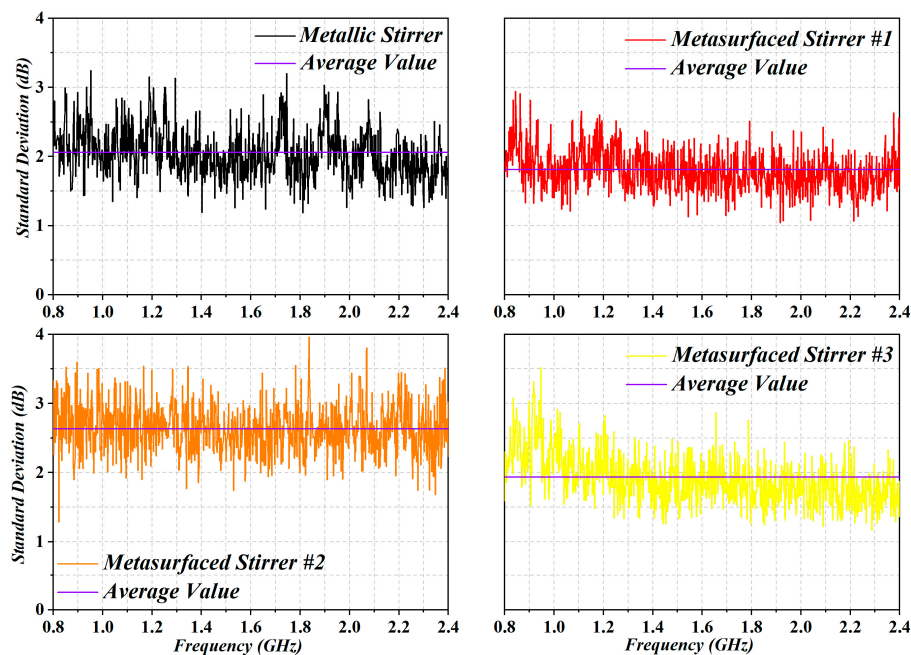


Figure 6. Standard deviation with respect to the mean value of maximum simulated obtained by each of the 12 steps, for a complete rotation of the stirrer.

## 2. Conclusions

In this paper, we have analyzed the effects of introducing different types of metasurface stirrers in reverberation chambers, compared to the traditional metallic stirrer. Three metasurface stirrers have been studied: one with two unit cells arranged alternatively (#1), another one with two unit cells arranged in a chessboard-like manner (#2), and a third one with two unit cells in random arrangement (#3). From the correlation coefficient and TSCS results obtained, we can conclude that the field uniformity is somehow improved for the RC with metasurfaced stirrer #1. Since this stirrer is

comprised of a metasurface with negligible volume (as compared to a metallic stirrer), the test volume of the RC is significantly extended. The volume extension is dependent on the dimensions of the mechanical stirrer.

**Author Contributions:** H.S., F.M., and C.G. conceived the idea and wrote the present manuscript. The simulations were carried out by H.S., M.W., J.S., B.X., K.W., X.D., Q.X., and Z.L. All the authors participated in discussions relevant to the presented sensing system.

**Funding:** This research was funded by [National Natural Science Foundation of China] grant number [61501227, 61071019], [Six talent peaks project in Jiangsu Province] grant number [GDZB-009], [Foundation of Key Laboratory of Radar Imaging and Microwave Photonics, NUAA, Ministry of Education] grant number [XCA17001-05], [Postdoctoral Science Foundation of China] grant number [2015M581789], [56YAH17032 of NUAA], [Jiangsu Innovation Program for Graduate Education] grant number [KYLX16-0370], [Fundamental Research Funds for the Central Universities] grant number [NJ20160011], [MINECO-Spain] grant number [TEC2016-75650-R], [Generalitat de Catalunya] grant number [2017SGR-1159] and FEDER funds, the [Foundation of Graduate Innovation Center in NUAA] grant numbers [kfj20170414, kfj20170411], and support from the Fundamental Research Funds for the Central Universities.

**Acknowledgments:** Hengyi Sun acknowledges the China Scholarship Council (CSC) for Grant 201706830064. Zhuo Li acknowledges the financial support from National Natural Science Foundation of China under Grant No.61871215.

**Conflicts of Interest:** The authors declare no conflict of interest. The funders had no role in the design of the study; in the collection, analyses, or interpretation of data; in the writing of the manuscript; or in the decision to publish the results.

## References

1. Wu, D.I.; Chang, D.C. The effect of an electrically large stirrer in a mode-stirred chamber. *IEEE Trans. Electromagn. Compat.* **1989**, *31*, 164–169. [[CrossRef](#)]
2. Serra, R.; Leferink, F. Optimizing the stirring strategy for the vibrating intrinsic reverberation chamber. In Proceedings of the 9th International Symposium on EMC and 20th International Wroclaw Symposium on Electromagnetic Compatibility, Wroclaw, Poland, 13–17 September 2010.
3. Clegg, J.; Marvin, A.C.; Dawson, J.F.; Porter, S.J. Optimization of stirrer designs in a reverberation chamber. *IEEE Trans. Electromagn. Compat.* **2005**, *47*, 824–832. [[CrossRef](#)]
4. Bruns, C. Three-Dimensional Simulation and Experimental Verification of a Reverberation Chamber. Ph.D. Thesis, Swiss Federal Institute of Technology in Zurich (ETH Zurich), Zurich, Switzerland, 2005.
5. Moglie, F.; Primiani, V.M. Analysis of the independent positions of reverberation chamber stirrers as a function of their operating conditions. *IEEE Trans. Electromagn. Compat.* **2011**, *53*, 288–295. [[CrossRef](#)]
6. Clegg, J. Optimization of stirrer designs in a reverberation chamber. *IEEE Trans. Electromagn. Compat.* **2002**, *44*, 442–457. [[CrossRef](#)]
7. Plaza-González, P.; Monzó-Cabrera, J.; Catalá-Civera, J.M.; Sánchez-Hernández, D. Effect of mode-stirrer configurations on dielectric heating performance in multimode microwave applicators. *IEEE Trans. Microw. Theory Tech.* **2005**, *53*, 1699–1706. [[CrossRef](#)]
8. Lundén, O.; Wellander, N.; Bäckström, M. Stirrer blade separation experiment in reverberation chambers. In Proceedings of the 2010 IEEE International Symposium on Electromagnetic Compatibility, Fort Lauderdale, FL, USA, 25–30 July 2010.
9. Pfennig, S.; Krauthäuser, H.G. Comparison of methods for determining the number of independent stirrer positions in reverberation chambers. In Proceedings of the 2013 International Symposium on Electromagnetic Compatibility, Brugge, Belgium, 2–6 September 2013.
10. Pfennig, S.; Krauthäuser, H.G.; Moglie, F.; Primiani, V.M. A continued evaluation of the general method for determining the number of independent stirrer positions in reverberation chambers. In Proceedings of the 2014 International Symposium on Electromagnetic Compatibility, Gothenburg, Sweden, 1–4 September 2014.
11. Sun, H.; Li, Z.; Gu, C.; Xu, Q.; Chen, X.; Sun, Y.; Lu, S.; Martin, F. Metasurfaced reverberation chamber. *Sci. Rep.* **2018**, *8*, 1577. [[CrossRef](#)] [[PubMed](#)]
12. Cui, T.J.; Qi, M.Q.; Wan, X.; Zhao, J.; Cheng, Q. Coding metamaterials, digital metamaterials and programmable metamaterials. *Light: Sci. Appl.* **2014**, *10*, e218. [[CrossRef](#)]

13. Sun, H.; Gu, C.; Li, Z.; Xu, Q.; Song, J.; Xu, B.; Dong, X.; Wang, K.; Martín, F. Enhancing the number of modes in metasurfaced reverberation chambers for field uniformity improvement. *Sensors* **2018**, *18*, 3301. [[CrossRef](#)] [[PubMed](#)]
14. Sun, H.; Gu, C.; Chen, X.; Li, Z.; Liu, L.; Xu, B.; Zhou, Z. Broadband and broad-angle polarization-independent metasurface for radar cross section reduction. *Sci. Rep.* **2017**, *7*, 40782. [[CrossRef](#)] [[PubMed](#)]
15. Lunden, O.; Backstrom, M. Stirrer efficiency in FOA reverberation chambers. Evaluation of correlation coefficients and chi-squared tests. In Proceedings of the IEEE International Symposium on Electromagnetic Compatibility. Symposium Record (Cat. No.00CH37016), Washington, DC, USA, 21–25 August 2000.
16. Hill, D.A. Plane wave integral representation for fields in reverberation chambers. *IEEE Trans. Electromagn. Compat.* **1998**, *40*, 209–217. [[CrossRef](#)]
17. Hill, D.A. *Electromagnetic Fields in Cavities: Deterministic and Statistical Theories*, 1st ed.; John Wiley & Sons, Inc.: Hoboken, NJ, USA, 2009; ISBN 978-0-470-46590-5.
18. El Baba, I.; Lalléchère, S.; Bonnet, P.; Benoit, J.; Paladian, F. Computing total scattering cross section from 3-D reverberation chambers time modeling. In Proceedings of the 2012 Asia-Pacific Symposium on Electromagnetic Compatibility, Singapore, 21–24 May 2012.
19. Xu, Q.; Huang, Y.; Xing, L.; Tian, Z.; Stanley, M.; Yuan, S. B-scan in a reverberation chamber. *IEEE Trans. Antennas Propag.* **2016**, *64*, 1740–1750. [[CrossRef](#)]
20. Xu, Q.; Huang, Y.; Xing, L.; Tian, Z.; Song, C.; Stanley, M. The limit of the total scattering cross section of electrically large stirrers in a reverberation chamber. *IEEE Trans. Electromagn. Compat.* **2016**, *58*, 623–626. [[CrossRef](#)]
21. Lerosey, G.; de Rosny, J. Scattering cross section measurement in reverberation chamber. *IEEE Trans. Electromagn. Compat.* **2007**, *49*, 280–284. [[CrossRef](#)]
22. Hill, D.A.; Ma, M.T.; Ondrejka, A.R.; Riddle, B.F.; Crawford, M.L.; Johnk, R.T. Aperture excitation of electrically large, lossy cavities. *IEEE Trans. Electromagn. Compat.* **1994**, *36*, 169–178. [[CrossRef](#)]
23. Genender, E.; Holloway, C.L.; Remley, K.A.; Ladbury, J.M.; Koepke, G.; Garbe, H. Simulating the multipath channel with a reverberation chamber: Application to bit error rate measurements. *IEEE Trans. Electromagn. Compat.* **2010**, *52*, 766–777. [[CrossRef](#)]
24. Holloway, C.L.; Shah, H.A.; Pirkel, R.J.; Remley, K.A.; Hill, D.A.; Ladbury, J. Early time behavior in reverberation chambers and its effect on the relationships between coherence bandwidth, chamber decay time, RMS delay spread and the chamber buildup time. *IEEE Trans. Electromagn. Compat.* **2012**, *54*, 714–725. [[CrossRef](#)]
25. CISPR, Joint Task Force A–IEC SC 77B, IEC 61000-4-21 Electromagnetic Compatibility (EMC)-Part 4-21: Testing and Measurement Techniques-Reverberation Chamber Test Methods. International Electrotechnical Commission (IEC) International Standard, 2011. Available online: <https://webstore.iec.ch/publication/4191#additionalinfo> (accessed on 5 September 2018).

